Rare Metal Materials and Engineering
Volume 48, Issue 2, February 2019
Available online at www.rmme.ac.cn

Science Press

Cite this article as: Rare Metal Materials and Engineering, 2019, 48(2): 0366-0374.

ARTICLE

Effect of Strain Amplitude on Cyclic Deformation Behavior of Nickel-Based Single Crystal Superalloy DD11 in Low Cycle Fatigue

Guo Yuanyuan[1,2], Zhao Yunsong[2], Zhang Jian[2], Liu Yanfei[1,2], Luo Yushi[2], Sha Jiangbo[1]

[1] Beihang University, Beijing 100191, China; [2] Science and Technology on Advanced High Temperature Structural Materials, Beijing Institute of Aeronautical Materials, Beijing 100095, China

Abstract: The cyclic stress response behavior and failure modes of nickel-based single crystal superalloys DD11 with [001] orientation in low cycle fatigue at 980 ºC and strain amplitude range of 0.5%~1.2% were investigated. The relationship between deformation microstructure and fatigue behavior was established. The results show that cyclic softening occurs and the softening degree decreases with increasing the strain amplitude. The coarsening of γ' and the broadening of transverse channels of γ are liable to cause the movement of dislocation in the γ channel and result in cyclic softening. Moreover, the dislocation recovery occurs at the low strain amplitude, which also causes cyclic softening. The pilling-up of dislocation occurs at the γ/γ' interfaces as the degree of coarsening γ' and broadening transverse channels of γ decreases when the strain amplitude is large than 0.8%, which results in a decrease in the degree of cyclic softening. The fatigue failure mode changes from normal fracture to shear fracture, corresponding to the transition of crack from stable propagation to the instant fracture.

Key words: low cycle fatigue; strain amplitude; cyclic softening; fatigue fracture

Nickel-based single-crystal superalloys (SCs) are widely used as blade materials in gas turbines due to their excellent creep resistance, persistent strength and thermal fatigue resistance at the elevated temperature[1-3]. Nevertheless, it is needed to consider the fatigue behavior of the turbine blade, especially in the platform region, where low cycle fatigue is one of the most common failure modes[4-7].

The strain amplitude is a key factor that dominates the low cycle fatigue life and fatigue mechanisms of disks or blade components made from Ni-based SCs, which may be subjected to the engine start-up and cooling-down at the moderate temperatures. It was confirmed that with increasing the strain amplitude, the density of dislocation increases[6] and the plastic deformation state and microstructure change completely from anisotropy to isotropy[8]. The cyclic stress response, including the cyclic hardening and cyclic softening, is related to dislocation or stacking fault that is dependent on the strain amplitude and fatigue testing temperatures [6]. Noteworthily, Li found that the slip bands can still be observed and the movement of dislocation is not homogeneous at 750 °C[9]. However, the understanding of the effect of strain amplitude on LCF behaviors of the Ni-based SCSs is still far from systematization.

The fatigue deformation mechanism is the key factor influencing the cyclic stress response behaviors and fatigue fracture of the Nickel-based SCs, and is governed by microstructure of alloy, loading condition and environment, etc[9-13]. The cyclic softening behavior is related to the coarsening of γ' under the fatigue loading conditions[14]. At elevated temperatures, the movement mode of dislocation is glide-climb[15], and the rapid generation of dislocation networks at the coarse γ/γ' interfaces may cause cyclic

Received date: February 14, 2018
Foundation item: National Natural Science Foundation of China (51471014)
Corresponding author: Sha Jiangbo, Ph. D., Professor, School of Materials Science and Engineering, Beihang University, Beijing 100191, P. R. China, Tel: 0086-10-82315989, E-mail: jbsha@buaa.edu.cn

softening[16,17].

When the temperature was low and the loading frequency was high, the failure of the SCs occurred at the {111} octahedral slip plane facet which was oblique to the direction of loading stress. On the contrary, the fatigue fracture was perpendicular to the loading direction, and then the failure mode changed from crystallographic to a non-crystallographic normal fracture type[18]. In addition, the morphology of the γ' phase could change the direction of crack propagation. The crack propagated along the γ channels or the γ/γ' interfaces when the γ/γ'-rafts was perpendicular to the stress axis in CMSX-4 and CMSX-6 alloys at 1050 °C[19].

DD11 is a novel second generation Nickel-based SCs which will be used for the blades and vanes in gas turbine engine. Some mechanical properties under tension and creep have been obtained[20,21]. However, the low cycle fatigue properties have not been investigated systematically. In this paper, the objective is to investigate the fatigue deformation behaviors at 980 °C. The low cycle fatigue was performed by the total strain-controlled tests to understand the effect of strain amplitude on the fatigue life, stress response, microstructural evolution and fracture modes.

1 Experiment

The nominal chemical composition of DD11 is listed in Table 1. The cylinders with [001] orientation, 15 mm in diameter and 170 mm in length, were prepared by the high rapid solidification method with a withdrawal rate of 3 mm·s^{-1}. The cylinders were heat treated at 1315 ºC for 6 h, and then aged at 1130 ºC for 4 h and 870 ºC for 24 h.

The specimens with a diameter of 6 mm were used for the low cycle fatigue tests. The orientation of the test bar deviating from [001] was within 8°, which was determined by the X-ray backscattering Laue method. The tests were conducted by the MTS (Material Test System) servo hydraulic testing machine under the total strain-range-control mode in air at 980 ºC. The strain ratio R was −1 and the strain amplitudes ($\Delta\varepsilon/2$) were 0.5%, 0.6%, 0.7%, 0.8%, 1.0%, 1.2%, which were controlled by an extensometer. The strain rate of all tests was 5×10^{-3} s^{-1}.

After the fatigue test, the microstructures of the longitudinal metallographic sections and the fatigue fracture surfaces were mechanically polished and chemically etched in a solution of 50 g $CuSO_4$+160 mL HCl+10 mL H_2SO_4+200 mL H_2O and observed using FEI-nano 450 scanning electron microscope (SEM). The fatigue fractured specimens were ultrasonically cleaned in a mixture of acetone and ethanol for 15~20 min. Transmission electron microscopy (TEM, JEM-2100F) was operated at a voltage of 200 kV to investigate the dislocation morphology. The TEM samples were taken from the transverse and longitudinal sections of the tested specimens by conventional grinding and twin-jet in a solution of 90% C_2H_5OH+10% $HClO_4$ at –20 °C.

Table 1 Chemical composition of the DD11 (wt%)

Cr	Co	W	Mo	Ta	Re	Al	Hf	B	C	Ni
4	8	7	2	7	3	6	0.2	0.1	0.1	Bal.

2 Results

2.1 Cyclic stress response behavior

Fig.1 shows various cyclic stress response behaviors at the $\Delta\varepsilon/2$ values from 0.5% to 1.2%. It was found that the cyclic stress response, including the cyclic softening and stability, is closely related to the strain amplitude in this work. The degree of the cyclic softening decreased progressively as the strain amplitude increased. At $\Delta\varepsilon/2$ of 0.5%, the alloy exhibited cyclic softening behavior, and the peak value of stress decreased from 500 MPa at the beginning stage to 400 MPa at the fracture time. At $\Delta\varepsilon/2$ of 0.8%, the alloy underwent cyclic hardening during the first 150 cycles, followed by cyclic softening till failure. This behavior is similar to the condition when $\Delta\varepsilon/2$ is 1.0%, indicating the cyclic hardening in the first 75 cycles and cyclic softening followed. When the $\Delta\varepsilon/2$ value was 1.2%, the alloy exhibited cyclic stability and the fatigue life decreased gradually. The coarsening of γ phase and the formation of dislocation networks are the most important roles for the softening behavior[14,16]. The stress amplitude rapidly decreases for all strain amplitudes, as a result of quick propagation of the crack when the fatigue fracture takes place.

2.2 Hysteresis loops of the alloy under LCF loading

The hysteresis loops at the $\Delta\varepsilon/2$ values from 0.5% to 1.2% are shown in Fig.2. The plastic strain energy was indicated by the area of the hysteresis loops at the half of fatigue life. It can be found that the area of hysteresis loops increases with the increasing strain amplitude. The LCF life of superalloys at high temperatures can be expressed by Coffin-Manson relationship as shown in Eq.(1):

$$\Delta\varepsilon_p/2=\varepsilon_f(2N_f)^c \quad (1)$$

where ε_f denotes the fatigue ductility coefficient, c is the fatigue ductility index and the N_f is the fatigue life. Thus, the fatigue life is prolonged as the plastic strain amplitude decreases.

2.3 Deformed microstructures of the alloy after LCF process

Fig.3 shows the deformed microstructure near the fracture surfaces of the fatigued samples at the $\triangle\varepsilon/2$ values of 0.5% and 1.0%. It has been found that the slip bands usually disappear when the temperature is higher than 800 °C[9,22]. However, the slip bands still appear near the fracture surface of this DD11 alloy, indicating the inhomogeneous plastic deformation during the low cycle fatigue process at 980 °C. This morphology is available in the fatigued samples at other $\Delta\varepsilon/2$ values.

Fig.4 shows the morphologies in the longitudinal section of the samples at the $\Delta\varepsilon/2$ values of 0.5%, 0.8%, 1.0% and 1.2%. Oxidation layers formed on the sample surface and they

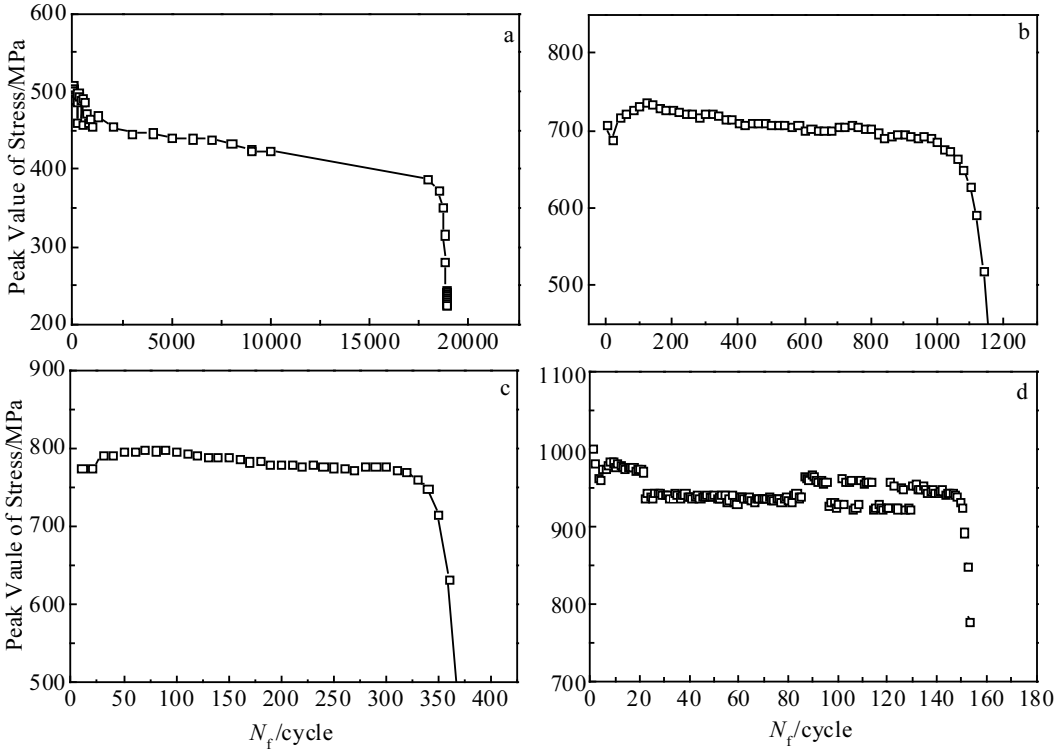

Fig.1 Cyclic stress response curves of the alloy at different strain amplitudes: (a) $\Delta\varepsilon/2$=0.5%, N_f=18 870; (b) $\Delta\varepsilon/2$=0.8%, N_f =1171; (c) $\Delta\varepsilon/2$=1.0%, N_f =374; (d) $\Delta\varepsilon/2$=1. 2%, N_f =158

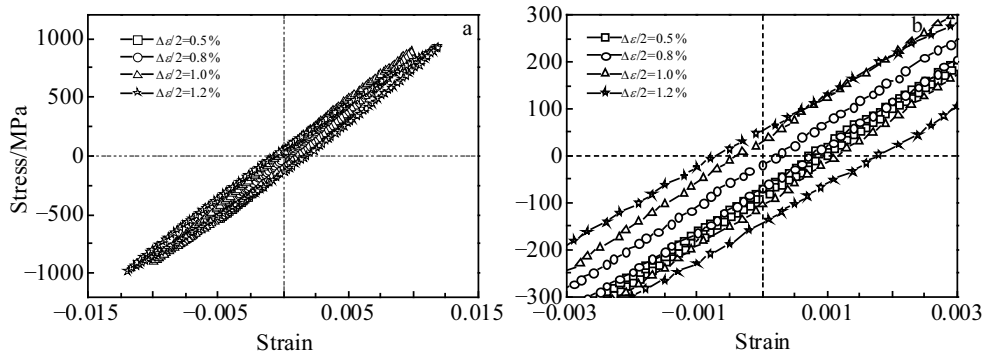

Fig.2 Hysteresis loops of the alloy under LCF loading at different strain amplitudes: (a) stress of –1000~1000 MPa and (b) stress of –300~300 MPa

became thicker as the $\triangle\varepsilon/2$ value decreased, i.e., the fatigue life increased. The multi-cracks starting from surface of the specimens were found to propagate predominantly perpendicular to the loading axis when the strain was lower than 1.2%, as observed in Fig.4a~4c. At the $\triangle\varepsilon/2$ value of 1.2%, a single crack propagated at an angle of 45° to the applied stress (Fig.4d).

Fig.5 exhibits the γ' morphology away from the fracture surface about 2 mm under different strain amplitudes. The γ' phase became coarser to some extent (Fig.5a, 5b and 5c) and its cubic degree decreased. When the $\triangle\varepsilon/2$ value was 0.5%, not only the γ' cubic degree droped sharply, but also the transverse channels of the γ phase broadened, as seen in Fig. 5d. As the $\triangle\varepsilon/2$ values were beyond 0.8%, the width of the transverse γ channels slightly increased, while the γ' cubic degree decreased a little.

Fig.6a~6c show the dislocation morphologies of the longitudinal sections of the fatigued samples at $\triangle\varepsilon/2$ of 0.5%. In this case, deformation zone only appeared in the γ channel and the dislocation density was low. The “zigzag” dislocation in the horizontal γ channel indicates that the cross-slip of the screw dislocation occurs on the {111} slip plane (Fig.6b). In addition, a climbing mechanism of dislocations moving within the γ phase was confirmed, as seen in Fig.6c, in which the

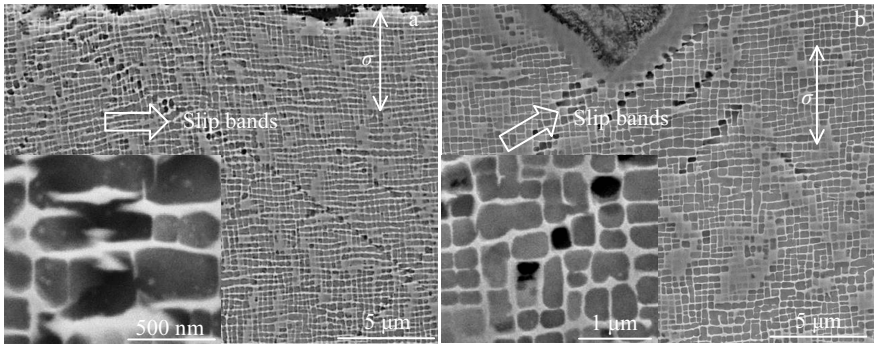

Fig.3 Slip bands of the longitudinal profile near the fatigue fracture surface of specimens: (a) $\Delta\varepsilon/2$=0.5%, N_f=18 870; (b) $\Delta\varepsilon/2$=1.0%, N_f=374

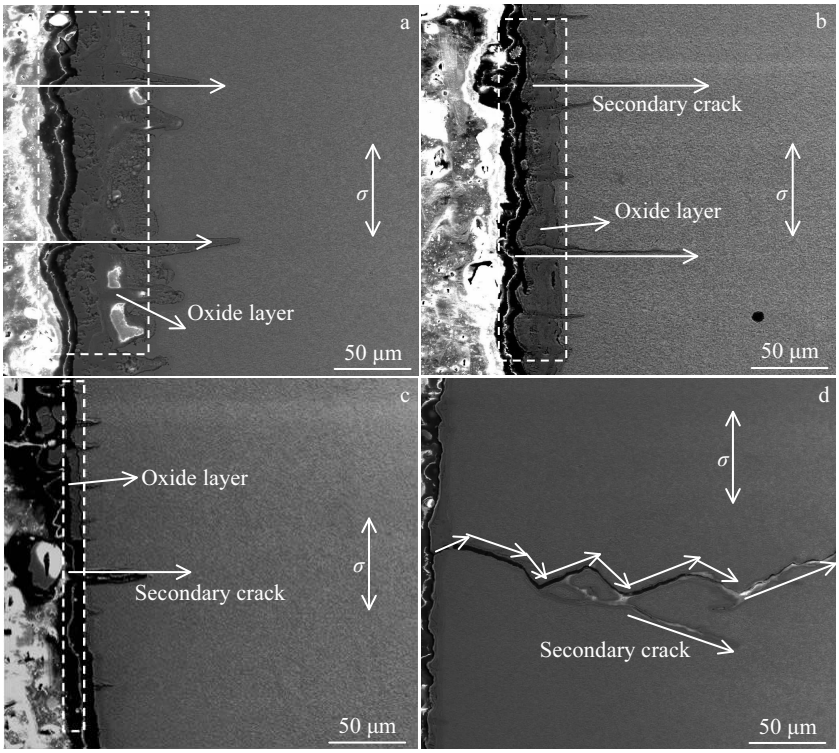

Fig.4 Oxide layer and secondary cracks near fatigue specimen surface: (a) $\Delta\varepsilon/2$=0.5%, N_f=18 870; (b) $\Delta\varepsilon/2$=0.8%, N_f=1171; (c) $\Delta\varepsilon/2$=1.0%, N_f=374; (d) $\Delta\varepsilon/2$=1.2%, N_f=158

bow-line dislocations appear around the γ' phase.

Fig.6d~6f show the characteristic of dislocation at$\Delta\varepsilon/2$ of 0.8%. It is noteworthy that the density of dislocation increased and the distribution of dislocation was homogeneous, as compared to the $\Delta\varepsilon/2$ value of 0.5% (Fig.6d). The irregular hexagonal dislocation network in the deformed zone was observed in Fig.6e and the dislocation loops were found bypassing the γ' phase through a mechanism of glide-climb (Fig.6f). The density of dislocations at the γ/γ' interface increased at the $\Delta\varepsilon/2$ values of 1.0% and 1.2% (see Fig.6g and 6h). The pilled-up dislocations at the interface and the homogeneous cross-slip of dislocation were the main dislocation morphologies as the $\triangle\varepsilon/2$ value was 1.2% (Fig.6i).

2.4 Fatigue fracture morphologies under different strain amplitudes

The fracture morphologies of the specimens were different under various total strain amplitudes. The fatigue fracture morphologies shown in Fig.7a~7d can be divided into a fatigue source and a crack propagation region.

At $\Delta\varepsilon/2$ of 0.5%, the oxidation played an important role in crack initiation and propagation (Fig.7a′). The fatigue sources appeared at the margin of fracture surface which was flat and smooth and was connected by sliding steps. The macroscopic characteristic was relatively rough at the instant rupture region

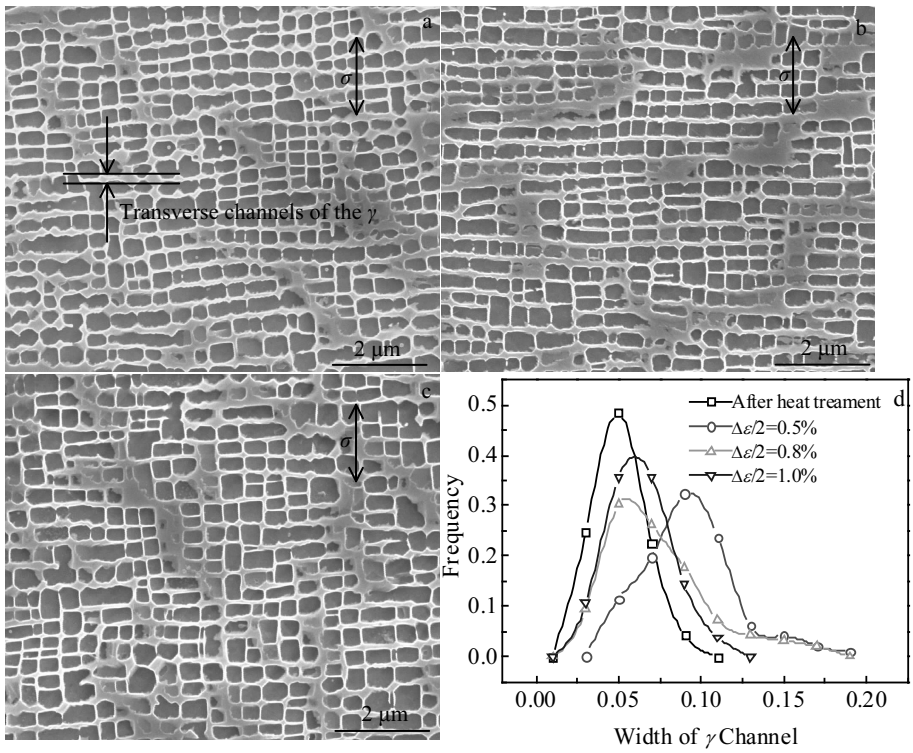

Fig.5 Microstructures of the longitudinal profile away from the fracture surface about 2 mm: (a) $\Delta\varepsilon/2$=0.5%, N_f=18 870; (b) $\Delta\varepsilon/2$=0.8%, N_f=1171; (c) $\Delta\varepsilon/2$=1.0%, N_f=374; (d) width of the transverse channels of the γ phase

due to the severe oxidation. When the $\Delta\varepsilon/2$ value was 0.8%, the spalling of oxide layer caused the crack initiation (Fig.7b′) and the instant region consisted of the cleavage-like faces (Fig.7b). As the $\Delta\varepsilon/2$ value was 1.0%, the fatigue source appeared at various positions of the fracture surface and the oxidation was also the most important reason for crack initiation (Fig.7c′). It is clear that the instant region was composed of the slip stage and the cleavage plane (Fig.7c). At the $\Delta\varepsilon/2$ value of 1.2%, the failure morphologies including fatigue and dimple were different from those of the $\Delta\varepsilon/2$ values in the range of 0.5% to 1.0%. The micro-porosity caused the crack initiation (Fig.7d′) and the area of the fatigue sources was 5% of the fracture surface, much lower than at other $\Delta\varepsilon/2$ values. The fatigue crack propagation region almost disappeared and the instant region showed that the radial feature terminated at the boundary of square-like area.

Fig.8 shows the morphology of the crack propagation region. The fatigue striation was not observed at a $\Delta\varepsilon/2$ of 0.5% as the crack propagation region was severely oxidized. The width of the fatigue striation gradually increased from about 9 μm for $\Delta\varepsilon/2$=0.7% to 60 μm for $\Delta\varepsilon/2$=0.8% and 75 μm for $\Delta\varepsilon/2$=1.0%.

3 Discussion

In this work, the cyclic stress response behaviors and the fatigue failure modes were different as the strain amplitude changed during the fatigue tests. The cyclic softening behavior was related to the interaction of dislocation-dislocation and the dislocation-precipitate. The oxidation and resolved shear stress intensity parameter were the main reasons to cause different failure modes. The following section will discuss the deformation microstructure and the dislocation to explain the cyclic stress response behavior and failure modes.

3.1 Cyclic softening for different stain amplitudes

The cyclic softening behavior dependent on the strain amplitudes was related to the γ' evolution and the movement of dislocation (Fig.1). At room temperature, the γ' was a softer phase. As the temperature increased, the hardness of γ and γ' changed gradually but the γ became the softer phase, and the dislocation movement was hindered by harder γ' phase[23]. Thus, the dislocation disappeared at the γ' phase and bowed out around the γ' phase (Fig.6).

It is well known that the cubic γ' phase can well hinder the slipping of dislocations in the γ channel[1-24]. In this work, however, the γ' phase became coarser and its cubic degree decreased, which caused the interfacial misfit stress and the coherency stress which decreased during LCF at 980 °C (Fig.5). As a result, the Orowan stresses of dislocation decreased due to the coarsening of γ' phase and the dislocations bowed into

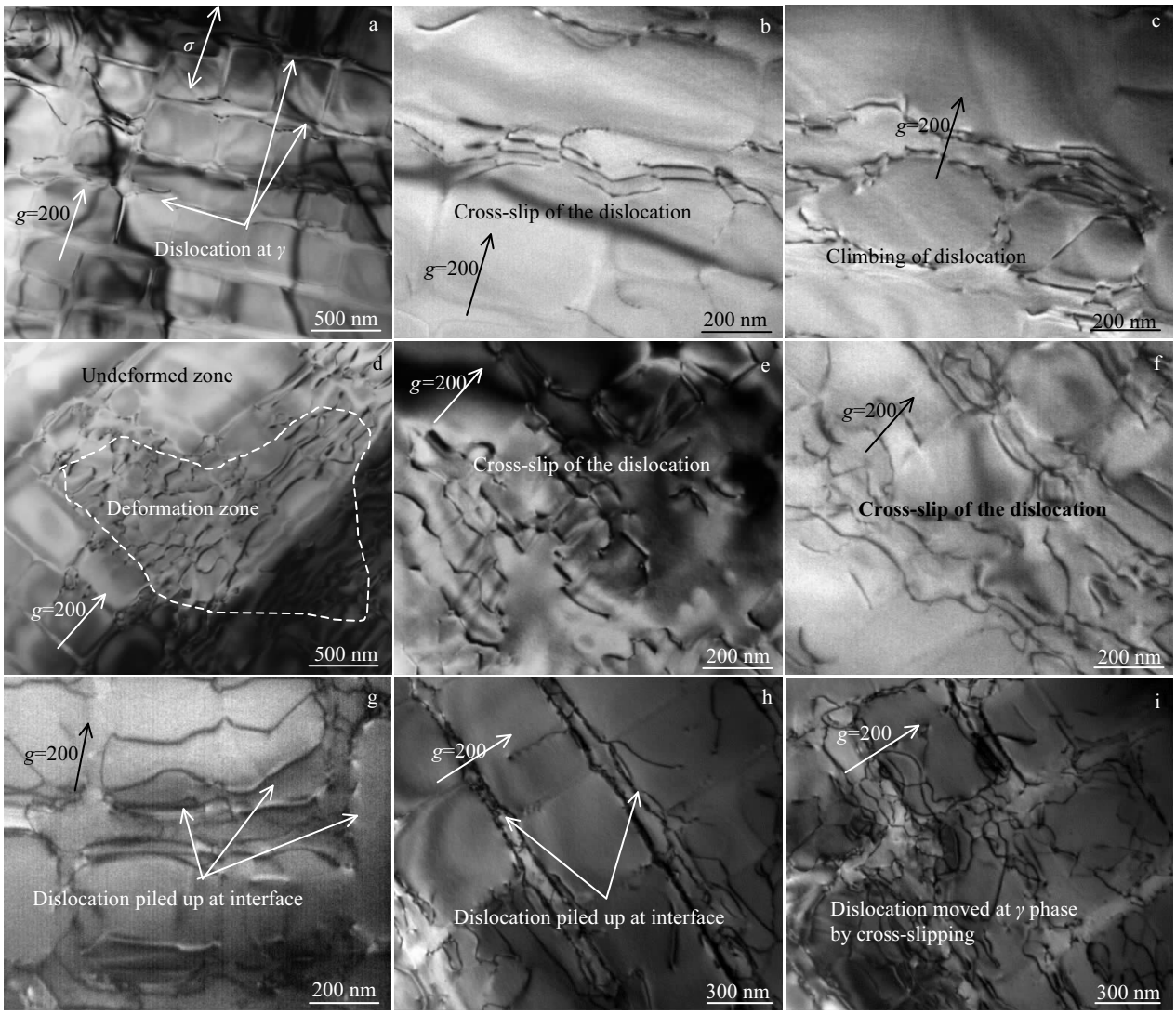

Fig.6 Dislocation configurations of the DD11 alloys after LCF failure under different strain amplitudes: (a~c) $\Delta\varepsilon/2$=0.5%, N_f =18 870; (d~f) $\Delta\varepsilon/2$=0.8%, N_f =1171; (g) $\Delta\varepsilon/2$=1.0%, N_f =374; (h, i) $\Delta\varepsilon/2$=1.2%, N_f =158

the γ phase. Moreover, the width of the γ channel increased in a direction vertical to the axial of stress (Fig.5d). These morphologies suggest that the movement of dislocation in cross-slip and climb modes in the γ channel is easy (Fig.6), subsequently resulting in the cyclic softening of the DD11 alloy.

Noteworthily, the density of dislocation was low and the dislocations bypassed the γ' phase by climbing at the strain amplitude of 0.5% (Fig.6c). This confirms that the recovery of the dislocation occurs, which is also responsible for the cyclic softening. When the $\Delta\varepsilon/2$ value increased, numerous dislocations piled up at the γ/γ' interface and the density of dislocation increased (Fig.6g and 6h). The addition of Re may increase the lattice mismatch and the interface strength[16]. The follow-up dislocations can be hindered strongly by those dislocations blocked by the γ/γ' interface. As a result, the cyclic softening degree decreased with increasing the strain amplitude (Fig.1).

3.2 Failure modes under different stain amplitudes

The failure modes changed from a normal fracture characteristic (which was perpendicular to the loading direction) to a shear fracture characteristic (which was oblique to the loading direction) during LCF at 980 °C (Fig.7). The oxidation degree and the resolved shear stress intensity parameter dominated this failure mode transition[24]. In the $\triangle\varepsilon/2$ range of 0.5%~1.0%, the failure mode was a normal fracture followed by shear fracture. The surface of specimen was oxidized and the crack in the fatigue source area mainly propagated in the perpendicular direction to the loading axis (Fig.4a, 4b and 4c). At the beginning of crack propagation, the crack tip might also be oxidized, which accelerated the crack growth rate, while the loading stress was low and the length of

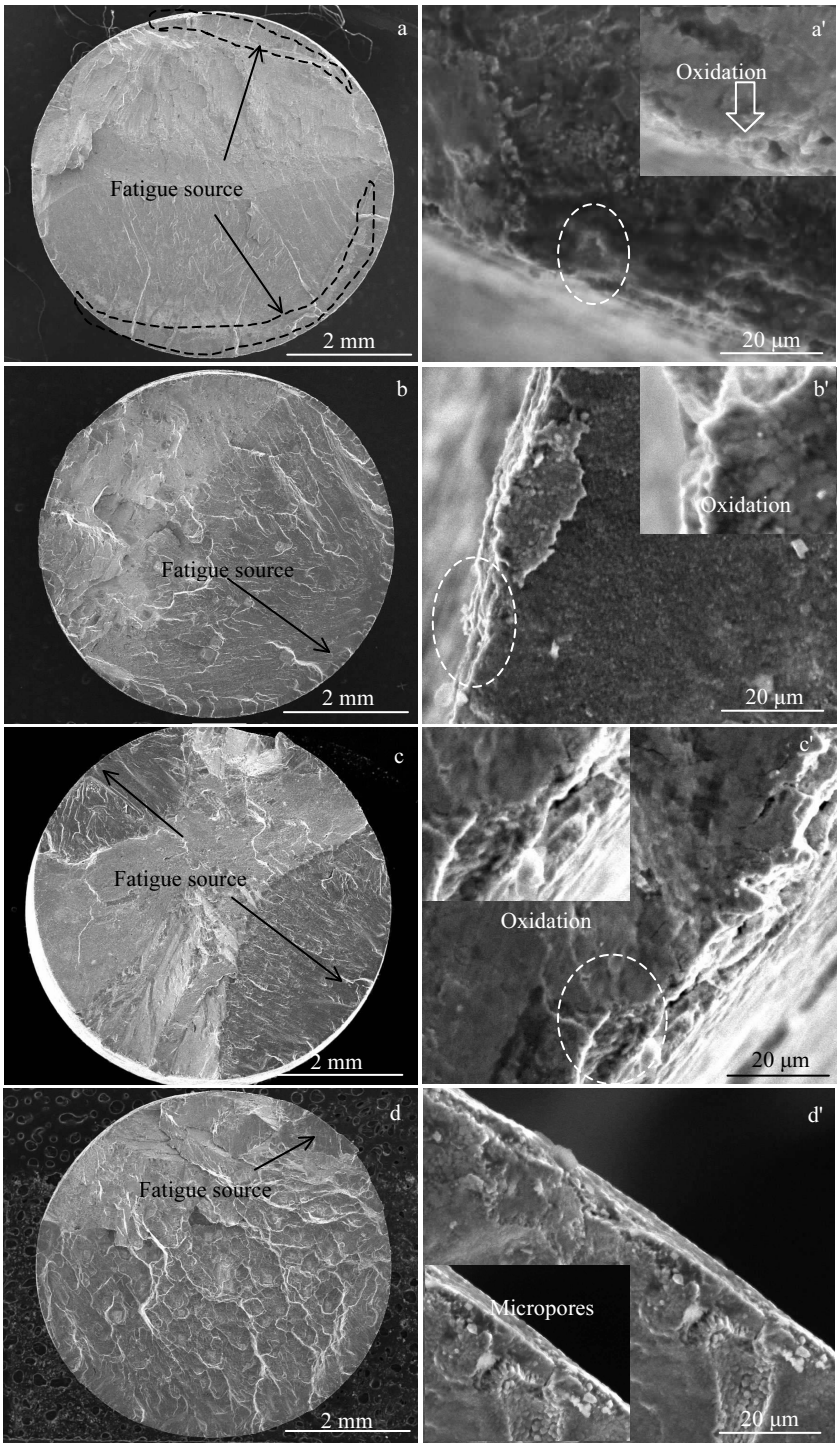

Fig.7 Characteristics of fatigue surface under different strain amplitudes: (a, a') $\Delta\varepsilon/2$=0.5%, N_f =18 870; (b, b') $\Delta\varepsilon/2$=0.8%, N_f =1171; (c, c') $\Delta\varepsilon/2$=1.0%, N_f =374; (d, d') $\Delta\varepsilon/2$=1.2%, N_f =158

the crack was short at this moment. In this case, the pene- tration depth of oxygen per cycle was greater than the crack increment per cycle and the embrittling effect by the oxidation determined the crack growth[18,25]. In the instant region, the length of crack was long enough so that the resolved shear stresses intensity parameter and the crack growth rate were higher. Thus the resolved shear stresses played a key role in the process of crack growth and behaved the shear fracture with a cleavage-like morphology in the instant region. When the strain amplitude was 1.2%, the loading and the resolved shear stress intensity parameter were higher enough, so the cracks always propagated by the shear fracture, leaving dimples on the fracture surface.

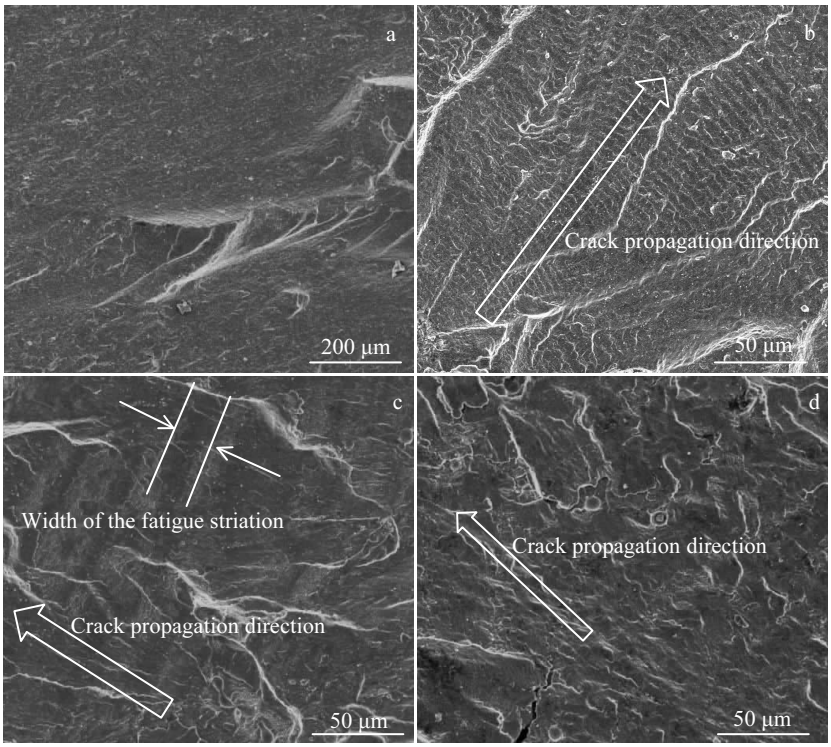

Fig.8 Characteristics of fatigue propagation region: (a) $\Delta\varepsilon/2$=0.5%; (b) $\Delta\varepsilon/2$=0.7%; (c) $\Delta\varepsilon/2$=0.8%; (d) $\Delta\varepsilon/2$=1.0%

4 Conclusions

1) The cyclic stress response behavior of the DD11 alloy is closely related to the strain amplitude level. The cyclic softening degree decreases progressively as the strain amplitude increases.

2) With increasing the strain amplitude, the cyclic softening degree decreases due to the increase in the density of dislocation, and the distribution of dislocation becomes homogeneous. The follow-up dislocations can be strongly hindered by dislocations that is blocked by γ/γ' interface.

3) The fatigue failure mode changes from the normal fracture mode to the shear fracture, corresponding to the transferring of stable propagation to instant fracture of the crack at 980 °C. The oxidation is the most important reason of the initiation of fatigue sources at the strain amplitudes less than 1%, while the porosity results in the crack initiation at the strain amplitude of 1.2%.

References

1 David K H, Laughlin E. *Physical Metallurgy, Volume III-Fifth Edition*[M]. New York: Elsevier, 2014: 2305

2 Reed R C. *Superalloys: Fundamentals and Applications*[M]. Cambridge UK: Cambridge University Press, 2006: 121

3 Pollock T M. *Nature Materials*[J], 2016, 15(8): 809

4 Pineau A, McDowell D L, Busso E P *et al. Acta Materialia*[J], 2016, 107: 484

5 Gallardo J M, Rodríguez J A, Herrera E J. *Wear*[J], 2002, 252 (3-4): 264

6 Zhang P, Zhu Q, Hu C *et al. Materials & Design*[J], 2015, 69: 12

7 Zhang W J. *Materials Science and Engineering A*[J], 2016, 650: 389

8 Brien V, Décamps B., *Materials Science and Engineering A*[J], 2001, 316(1-2): 18

9 Li P, Li Q Q, Jin T *et al*. *International Journal of Fatigue*[J], 2014, 63(1):137

10 Reed P A S. *Materials Science and Technology*[J], 2013, 25(2): 258

11 Defresne A, Remy L. *Materials Science and Engineering A*[J], 1990, 129(1): 45

12 Antolovich S D *et al*. In: Bruce A S, Antolovich F, Stephen D eds. *Superalloys 1992*[C]. Warrendale, PA: the Minerals, Metals and Materials Society, 1992: 39

13 Goswami T, Hanninen H. *Materials & Design*[J], 2001, 22(3): 217

14 Mark Harady *et al.* In: Jiang R, Gao N, Ward M eds. *Superalloys 2016*[C]. Warrendale, PA: the Minerals, Metals and Materials Society, 2016: 908

15 Yu J J, Sun X F, Jin T *et al. Materials Science and Engineering A*[J], 2010, 527: 2379

16 Marchionni M, Osinkolu G A, Onofrio G. *International Journal of Fatigue*[J], 2002, 24(12): 1261

17 Phillips P J, Unocic R R, Kovarik L *et al*. *Scripta Materialia*[J], 2010, 62(10): 790

18 Telesman J, Ghosn L J. *Journal of Engineering for Gas Turbines and Power*[J], 1996, 118(2): 399
19 Ott M, Mughrabi H. *Materials Science and Engineering A*[J], 1999, 272(1): 24
20 Mark Harady *et al.* In: Zhao Y S, Zhang J, Luo Y S eds. *Superalloys 2016*[C]. Warrendale, PA: The Minerals, Metals and Materials Society, 2016: 683
21 Zhao Y S, Zhang J, Luo Y S *et al. Materials Science and Engineering A*[J], 2016, 672: 143
22 Zhou D, Moosbrugger J C, Jia Y *et al*. *International Journal of Plasticity*[J], 2005, 21(12): 2344
23 He M Y, Evans A G. *Acta Materialia*[J], 2010, 58(2): 583
24 Liu L, Meng J, Liu J L *et al*. *Materials & Design*[J], 2017, 131: 441
25 Pollock T M *et al*. In: Connolley T, Connolley T, Reed P A S eds. *Superalloys 2000*[C]. Warrendale, PA: The Minerals, Metals and Materials Society, 2000: 435

应变幅对第二代镍基单晶高温合金 DD11 980 ℃低周疲劳性能的影响

郭媛媛[1,2]，赵云松[2]，张　剑[2]，刘砚飞[1,2]，骆宇时[2]，沙江波[1]
(1. 北京航空航天大学，北京 100191)
(2. 北京航空材料研究院 先进高温结构材料重点实验室，北京 100095)

摘　要：通过对第二代镍基单晶高温合金 DD11 在 980 ℃条件下低周疲劳性能测的试及表征，研究了不同应变幅（$\Delta\varepsilon/2$=0.5%~1.2%）对循环应力响应行为和断裂模式的影响，建立了显微组织演变和疲劳行为之间的联系。结果表明，该合金发生了循环软化行为并且随着应变幅的提高，循环软化程度降低。γ'的粗化以及垂直于加载轴方向的 γ 通道加宽有利于位错运动的进行，因此造成了循环软化。当应变幅为 0.5%时，位错回复也是造成循环软化的原因。随着应变幅增加至 0.8%后，γ'的粗化以及垂直于加载轴方向的 γ 通道加宽程度降低，位错在两相界面上发生了塞积，造成了循环软化程度的降低。疲劳失效模式从扩展区的正断模式转变为了瞬断区的剪切断裂模式。本研究有利于建立单晶高温合金涡轮叶片疲劳失效模式、循环应力响应行为和组织三者的关系，对涡轮叶片的设计使用具有一定的指导意义。

关键词：低周疲劳；应变幅；循环软化；疲劳断裂

作者简介：郭媛媛，女，1993 年生，硕士生，北京航空航天大学材料科学与工程学院，北京 100191，电话：010-62498231，E-mail: guoyuanyuanjida@163.com